Effect of rock mass structure and block size on the slope stability

——Physical modeling and discrete element simulation

LI Shihai[1], LIAN Zhenzhong[1,2] & J. G. Wang[3]

1. Institute of Mechanics, Chinese Academy of Sciences, Beijing 100080, China;
2. Graduate School, Chinese Academy of Sciences, Beijing 100060, China;
3. Tropical Marine Science Institute, National University of Singapore, Singapore 119260
Correspondence should be addressed to Li Shihai (email: shli@imech.ac.cn)

Received June 15, 2004

Abstract This paper studies the stability of jointed rock slopes by using our improved three-dimensional discrete element methods (DEM) and physical modeling. Results show that the DEM can simulate all failure modes of rock slopes with different joint configurations. The stress in each rock block is not homogeneous and blocks rotate in failure development. Failure modes depend on the configuration of joints. Toppling failure is observed for the slope with straight joints and sliding failure is observed for the slope with staged joints. The DEM results are also compared with those of limit equilibrium method (LEM). Without considering the joints in rock masses, the LEM predicts much higher factor of safety than physical modeling and DEM. The failure mode and factor of safety predicted by the DEM are in good agreement with laboratory tests for any jointed rock slope.

Keywords: rock masses, slope stability, DEM simulation, block size effect, joints configuration effect, limit equilibrium method.

DOI: 10.1360/04zze1

Rock slope has many geological structures with different sizes, configurations and mechanical properties such as joints, fissures, faults, shear bands and so on[1]. These geological structures may make the slope unstable, producing toppling, fracturing or sliding failures. A lot of investigations have focused on the stability of jointed rock slope, however, the mechanisms on the progressive failure of jointed rock slope is still an open issue in either physical modeling or numerical simulation. Therefore it is necessary to acquire an apparent recognition of slope stability and failure mechanism by physical modeling and numerical simulation. Rock slopes are usually intersected by geological structures into blocks and the blocks are in different orientations. Sun[2] classifies the structures of rock mass into four types. He brought forward the following characteristics of block structures: (1) rock blocks are formed by the intersection of weak structural

interface; (2) the motion of rock blocks is governed by the configuration of structural interfaces, particularly continuous and straight interfaces; and (3) the mechanical properties of rock block are controlled by the continuous and straight structure interfaces, especially those weak structure interfaces. The failure mode of such rock blocks is sliding failure along weak structure interfaces.

Several numerical methods have been proposed to assess the stability of a rock slope and to describe the progressive failure. Limit equilibrium method (LEM) uses the factor of safety (FOS) to assess the stability of a rock slope[3,4]. The LEM assumes that a sliding surface is formed in the slope and the resistance force along the sliding surface achieves its limit state at any point. In order to consider inhomogeneous distribution of this resistance forces, the sliding body is divided into slice blocks. The resistance force at the bottom of each slice block is approximated by homogeneous force. Because the division of rock masses is purely geometrical, the slice blocks in LEM cannot include the effects of geological structures. LEM has been widely applied to the assessment of slope stability in engineering due to its simplicity[5]. However, it cannot describe the process of deformation and failure, and large-scale opening, fracturing, slipping, toppling, and rotating yet[6]. As pointed out by Jing[6], continuum-based numerical methods such as FEM and BEM confront big problems to treat the geological interfaces. An alternative is the discrete element method (DEM). The DEM is based on discontinuity analysis, thus easily describing sliding, toppling and rotating of rock blocks as well as the deformation and progressive failure process of slope without any difficulty. Two DEM models are prevailing: 3DEC corner-face model[7] and NURBM3D face-face model[8]. 3DEC uses corner-face contact for the interaction of two neighboring blocks. This model has been proved to be effective when interface takes place large structural deformation or rock block rotates heavily. It searches for contact in every time step, thus spending a lot of CPU time and requiring more storage space. Therefore, the corner-corner model is not suitable for a great number of rock blocks. In addition, the corner-corner contact cannot determine the direction and magnitude of contacting force and stress concentration may occur at the corner, producing fracture or "numerical locking". The NURBM3D face-face model[8] avoids the "numerical locking" and largely improves computational efficiency. Original face-face model cannot deal with block deformation. Recently, Li and his colleagues[9,10] improved the face-face model to include either rigid or deformable blocks.

Some experiments have been carried out to verify the prediction capability of discrete element methods. Barla et al.[11—13] studied the failure angle of barite and olefin block slope from both physical modeling and UDEC numerical simulation. Their physical modeling focused on the slope with straight joints. They gradually increased the inclination of the slope up to slipping. Their results show that, if the block size is 9 cm ×9 cm ×20 cm, the angle of failure is 38 degree by experimental measurement, while the UDEC predicted only 31 degree of failure angle. If the block size is 9 cm×9 cm×9 cm,

the angle of slope failure is 9 degree for experimental measurement and approximates 9 degree predicted by UDEC (this result is the same as the result obtained in this paper, see section 3). Based on the above results, they concluded that UDEC results are not always in agreement with experimental measurements even if the physical and geometrical parameters of a jointed rock slope are well known. This paper mainly focuses on the effect of rock mass structure and block size on the slope stability through physical modeling and numerical simulations with deformable face-face DEM model. The DEM simulations are also compared with the LEM simulations. As a result, safety factor obtained by LEM is much higher than both DEM and physical modeling for some jointed rock slopes.

1 Experiment setup for physical modeling

The experiment setup is shown in Fig. 1. This experiment is designed to study the failure modes of rock slopes with different joint configurations. This device is made of box for sample holder and pulley to incline the box until sliding. The box walls are made of transparent glass. From this glass, the sliding process can be recorded through digital or video camera. The wall is 20 mm thick and internal dimensions are 2000 mm×800 mm×1100 mm in length, width and height, respectively. A pulley is fixed on the upper front wall of the box to level the glass box when sample is prepared. The inclination is continued until the critical angle of a rock slope. Rock blocks are made from granite with three sizes: big (200 mm×100 mm×100 mm), middle (100 mm×100 mm×100 mm) and small (50 mm×50 mm×50 mm). The slope sample is prepared in the following procedure: First, lay a layer of big blocks and fix these blocks to the bottom and the sidewalls. Then put above layers according to the designated joint configuration. The slope of big blocks with straight joints is prepared as an example. Put six blocks in the width direction, five blocks in the length direction and five blocks in the height direction. Such a layout does not touch with the box wall. A thin layer of sands is put along the interface of blocks to smoothen the interface surface. Other four slopes are prepared in similar ways. When a slope is ready, incline the slope slowly through the pulley until slope slides or fails. Observe the deformation and failure process. The angle of the slope inclination when sliding or toppling occurs is the critical angle of the slope.

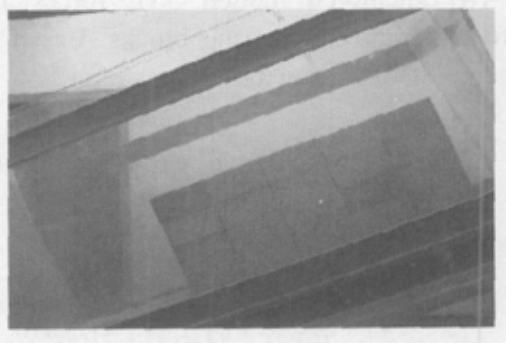

Fig. 1. Setup of experiments for slope stability.

2 Face-to-face contact three-dimensional discrete element method

2.1 Basic hypothesis

In this discrete element method, a rock slope is composed of blocks. These blocks

come from the intersection of rock masses by discontinuities such as joints, fissures. In order to describe the slope, face-to-face contact DEM has the following hypotheses:

a) Each block is deformable when external force is applied, and the motion of each block is governed by the Newton's second law of force and moment.

b) Interaction of two neighboring blocks is described by normal and tangential stiffness. Neighboring blocks embed each other. This equivalently puts virtual springs between rigid blocks. Therefore the deformation induced by block and joint can be easily decided. The normal and shear forces between neighboring blocks can be expressed by the spring deformation between the neighboring blocks, but they follow Mohr-Coulomb's law, too. No tension is allowed.

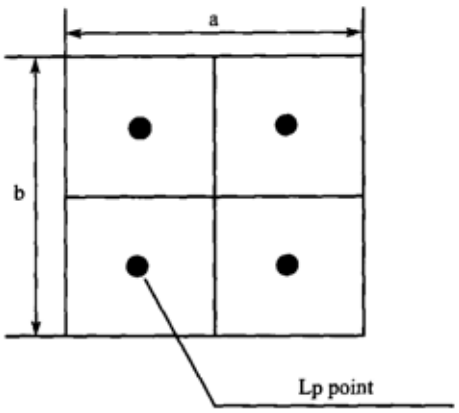

Fig. 2. Lp points for block contacting.

c) Each block face is divided into four equal areas to express the inhomogeneous force on interface and calculate moment of the block. The force in each area is assumed to be homogeneous and its force center is denoted as Lp (see Fig. 2).

2.2 Fundamental equations of block motions

Unlike continuum mechanics, DEM is based on the discontinuity analysis of discrete blocks, thus the compatibility of deformation along the interface of blocks is not mandatory. However, DEM must observe the equation of motion and physical equations.

(i) Equation of motion. The forces on each block have external force and contacting forces from neighboring blocks. Based on Newton's second law, each block has the equation of motion as

$$m_i\ddot{\vec{u}}_i + c_m\dot{\vec{u}}_i + c_k\sum_{j=1}^{n}(\dot{\vec{u}}_i - \dot{\vec{u}}_j) + k\sum_{j=1}^{n}(\vec{u}_i - \vec{u}_j) = \vec{F}, \tag{1}$$

and

$$I_i\ddot{\vec{\theta}}_i + c_I r_0^2\dot{\vec{\theta}}_i + c_k\sum_{k=1}^{n'}\{\vec{r}_k\times[\vec{r}_k\times(\dot{\vec{\theta}}_i - \dot{\vec{\theta}}_j)]\} + k\sum_{k=1}^{n'}\{\vec{r}_k\times[\vec{r}_k\times(\vec{\theta}_i - \vec{\theta}_j)]\} = \vec{M}, \tag{2}$$

where m_i, I_i are the mass and inertia of *i*th block, $\vec{u}_i$, $\dot{\vec{u}}_i$, $\vec{\theta}_i$, $\dot{\vec{\theta}}_i$ are the displacement, velocity, angular displacement and angular velocity, respectively. The subscripts '*j*' refers to the *j*th-neighboring block. *n* is the block number which is neighboring of the *i*th block, and n' the Lp points on the *i*th block. $\vec{F}$ is the external force such as gravity, and $\vec{M}$ the external moment. r_0 is the rotating radius and $\vec{r}_k$ the vector from mass

center to Lp point. c_I, c_m, c_k, k are physical constants.

(ii) Force-displacement relation (physical equation). The force-displacement relation at the Lp point is used to express the interaction of two blocks. When two blocks contact each other, this relationship can be expressed in the normal and tangential directions, respectively, as follows:

$$\begin{aligned} \Delta F_n &= -k_n A_s \Delta u_n, \\ \Delta F_s &= -k_s A_s \Delta u_s, \end{aligned} \tag{3}$$

where ΔF_n and ΔF_s are the increments of normal and tangential forces at the Lp point, and Δu_n and Δu_s the corresponding displacement increments. k_n and k_s are the normal and tangential stiffness, respectively, and A_s the area of the Lp zone. Eq. (3) is valid only when the blocks are in contact. When the interface is open ($F_n > \sigma_t^j A$), the forces on the interface are all zeros:

$$F_n = 0, \quad F_s = 0. \tag{4}$$

When the interface is sliding ($F_s > CA_s + F_n \tan\phi$), the forces on the interface observes the Mohr-Coulomb's law:

$$F_s = F_n \tan\phi + C, \tag{5}$$

where C is the cohesion and ϕ the frictional angle. F_n and F_s are the normal and tangential forces at the Lp point.

(iii) Block deformation. The block in the DEM is deformable. If the block material is linearly elastic, the stress-strain relation observes the Hooke's law:

$$\begin{Bmatrix} \varepsilon_{xx} \\ \varepsilon_{yy} \\ \varepsilon_{zz} \\ \gamma_{xy} \\ \gamma_{yz} \\ \gamma_{zx} \end{Bmatrix} = \frac{1}{E} \begin{bmatrix} 1 & -\mu & -\mu & 0 & 0 & 0 \\ -\mu & 1 & -\mu & 0 & 0 & 0 \\ -\mu & -\mu & 1 & 0 & 0 & 0 \\ 0 & 0 & 0 & 2(1+\mu) & 0 & 0 \\ 0 & 0 & 0 & 0 & 2(1+\mu) & 0 \\ 0 & 0 & 0 & 0 & 0 & 2(1+\mu) \end{bmatrix} \begin{Bmatrix} \sigma_{xx} \\ \sigma_{yy} \\ \sigma_{zz} \\ \tau_{xy} \\ \tau_{yz} \\ \tau_{zx} \end{Bmatrix}. \tag{6}$$

This equation is written in the following matrix form:

$$\{\varepsilon\} = [C]\{\sigma\}. \tag{7}$$

The displacement at any point inside the block can be obtained by intergrating eq. (7). In the local coordinate system, both rigid translation and rotation of the centroid are zero. Therefore, in the local coordinate the displacement in each block can be obtained:

$$u_{\text{local}} = \varepsilon_x x + \frac{\gamma_{xy}}{2} y + \frac{\gamma_{xz}}{2} z,$$

$$v_{\text{local}} = \varepsilon_y y + \frac{\gamma_{yz}}{2} z + \frac{\gamma_{yx}}{2} x, \tag{8}$$

$$w_{\text{local}} = \varepsilon_z z + \frac{\gamma_{zx}}{2} x + \frac{\gamma_{zy}}{2} y.$$

Finally, the displacement is

$$\begin{Bmatrix} u_{\text{local}} \\ v_{\text{local}} \\ w_{\text{local}} \end{Bmatrix} = \begin{Bmatrix} \frac{\sigma_{xx}}{E} - \frac{\mu}{E}(\sigma_{yy} + \sigma_{zz}) & \frac{\tau_{xy}}{2G} & \frac{\tau_{xz}}{2G} \\ \frac{\tau_{yx}}{2G} & \frac{\sigma_{yy}}{E} - \frac{\mu}{E}(\sigma_{xx} + \sigma_{zz}) & \frac{\tau_{yz}}{2G} \\ \frac{\tau_{zx}}{2G} & \frac{\tau_{zy}}{2G} & \frac{\sigma_{zz}}{E} - \frac{\mu}{E}(\sigma_{yy} + \sigma_{xx}) \end{Bmatrix} \begin{Bmatrix} x \\ y \\ z \end{Bmatrix}. \tag{9}$$

2.3 Coordinates, boundary condition and computation parameters

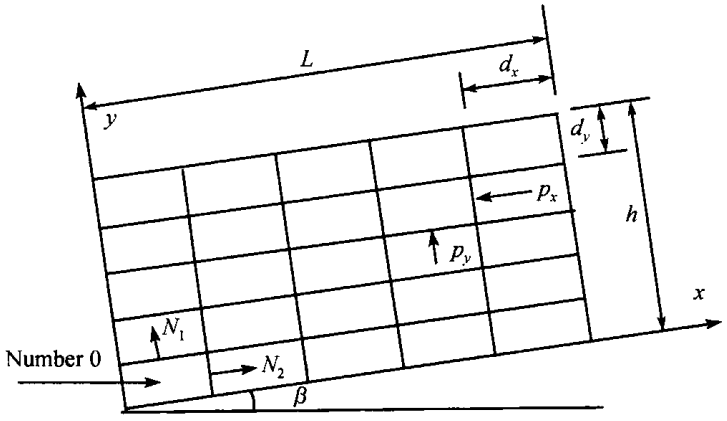

Fig. 3. Coordinates for straight jointed slope.

The coordinates used in computation are shown in Fig. 3. We will study domain of 2.0 m(L)×0.6 m(h)×1.2 m(Z). Except the fixed bottom layer, the upper layers do not contact with sidewalls. This slope has the following boundary conditions:

$$F_x = 0, \quad F_y = 0, \quad F_z = 0, \quad \text{when} \quad \begin{cases} x = 0, L, \\ y = h, \\ z = 0, L_Z, \end{cases} \tag{10}$$

and

$$u_x = 0, \quad u_y = 0, \quad \text{when} \quad y = 0. \tag{11}$$

The slope is intersected by three sets of structural planes. These planes are expressed as

$$\begin{cases} x = nd_x, \\ y = nd_y, \\ z = nd_z, \end{cases} \tag{12}$$

where N_1 and N_2 are two vectors in the normal direction, and their normal forces are P_x and P_y. L is the slope length and h the slope thickness. β is the slope angle. d_x, d_y, d_z are the dimensions of one block. n refers to the position of interface.

The frictional angle of interface is measured by the following experiment. Put one block on the fixed layer. Let the block sliding and measure the slope angle. This slope angle is the frictional angle of interface between blocks. The measured critical failure angles are almost the same for the three-size blocks. Table 1 summarizes the mechanical properties of rock blocks and joints. Table 2 is the geometrical properties of joints. These parameters are used in the DEM simulations.

Table 1 Mechanical properties of rock blocks and joints

Properties of blocks			Strength and stiffness of interface			
Density/kg·m^{-3}	Poisson ratio	E /N·m^{-2}	C/Pa	ϕ/(°)	k_n /N·m^{-3}	k_s/N·m^{-3}
2700	0.2	6.75×10^{10}	2.142	25.99	3.375×10^{11}	3.375×10^{11}

Table 2 Geometrical properties of joints

Joint set	Big block ($200\times100\times100$ mm^3)			Middle block ($100\times100\times100$ mm^3)			Small block ($50\times50\times50$ mm^3)		
	Space/m	Angle/(°)	Orient./(°)	Space/m	Angle/(°)	Orient./(°)	Space/m	Angle/(°)	Orient./(°)
1	0.2	90-β	0	0.1	90-β	0	0.05	90-β	0
2	0.1	90	90	0.1	90	90	0.1	90	90
3	0.1	β	180	0.1	β	180	0.1	β	180

3 Comparison of DEM results with experimental measurements

3.1 Failure angle of slope

First, we define case 1 for big blocks with straight joints, case 2 for big blocks with staged joints, case 3 for middle blocks with straight joints, case 4 for middle blocks with staged joints, and case 5 for mixed blocks. Failure angle refers to the critical slope angle when the slope just begins sliding. Table 3 compares the failure angle computed by DEM and experimental measurements. Generally, the DEM simulations are in good agreement with experimental measurements. Except case 3 of middle blocks with straight joints, failure angles are all among 21—23.5 degree for DEM and 19.5—26.3 degree for experimental measurement. For case 3, the failure angle calculated by DEM is still in the range of experimental measurements. This implies that the current DEM can correctly simulate the critical state of rock slopes regardless of joint distribution and block size. Block size and joint distribution do affect the failure angle of a jointed rock

Table 3 Comparison of failure angle between DEM and experiment

Methods	Case 1/(°)	Case 2/(°)	Case 3/(°)	Case 4/(°)	Case 5/(°)
Experiment	22.14—24 .2	25—26.3	9.8—11.6	23—24.9	19.5—21.8
DEM	23	25.5	10	23.5	21

slope. Their effects on failure modes and stress distribution will be discussed in subsequent sections.

3.2 Slope with straight continuous joints

(i) Failure modes. Cases 1 and 3 are straight continuous jointed slopes. Figs. 4 and 5 compare their failure modes observed in experiments and DEM simulations. Fig. 4 is for big blocks and Fig. 5 is for middle blocks. Experiments observe that the first front array rotates but the back arrays do not. This is toppling failure. DEM simulation can completely and accurately reproduce this failure mode. From the numerical simulation, mass center of each block moves to left downwards and at the same time, the block rotates in anti-clockwise direction. The assembly behaves toppling failure.

(ii) Stress distribution along sliding surface and vertical section. The stress distri-

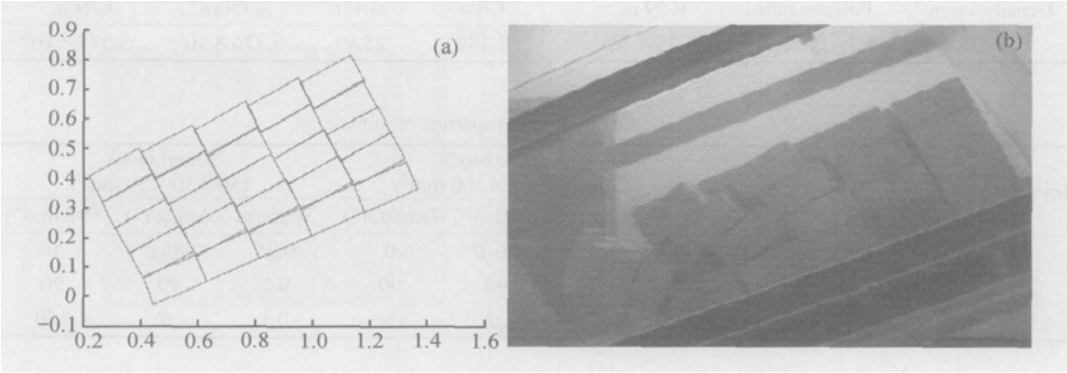

Fig. 4. Failure mode of slope with big blocks and straight joints. (a) DEM simulation; (b) experimental observation.

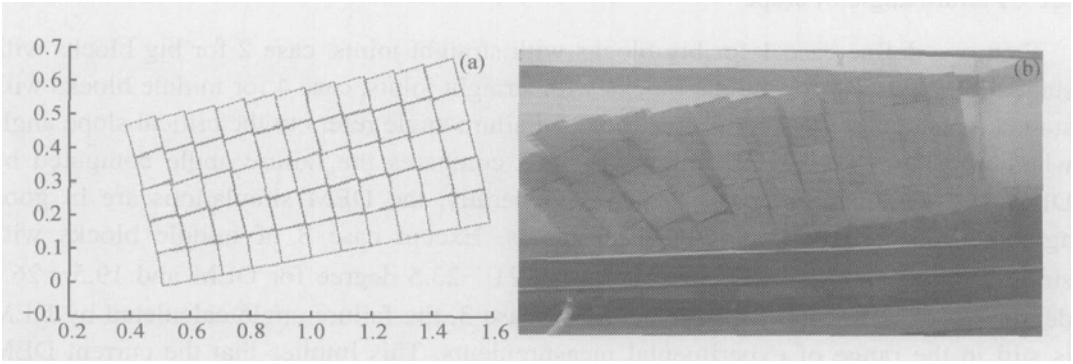

Fig. 5. Failure mode of slope with middle blocks and straight joints. (a) DEM simulation; (b) experimental observation.

bution is explored along the sliding surface and the vertical section or vertical joint. Fig. 6 is the distribution of normal force along the bottom layer (potential sliding surface) when the inclination of slope is at its critical angle. Because each block is divided into four equal size sub-blocks, the normal force achieves its maximum at the left-down corner and zero at the right-down corner. That means the block is rotating instead of sliding along the potential sliding surface. Furthermore, the result that $P_y/\rho gy'$ is always larger than 1 means the left-down corner burdens most of the self-weight due to the rotation of blocks. Fig. 7 shows the distribution of normal force when one block is divided into more than four sub-blocks in DEM computation. A stress concentration is observed at the left-down corner. If the strength of blocks is not enough, its left-down corner may be crushed. Therefore, the block may be crushed when the slope is rotating. Fig. 8 is the force distribution along section $x = 0.7$ m at critical angle. The force linearly decreases from over self-weight at the left-hand side while linearly increases from under self-weight at the right-hand side. The P_y finally approaches to the self-weight. This means that the contact of up-down blocks is loosing at the right side and tightening at the left side. The separation is observed at the right corner of up-bottom contact. Careful comparison shows that the block size has some effect on force distribution. The smaller the particle is, the stronger change the force has. This is due to the fact that bigger block is not easier to rotate in the slope. Their fitting equations are:

Left of big block and straight joint:

$$P_y / \rho gy' = 2.18 - 1.24\, y/h, \tag{13}$$

Right of big block and straight joint:

$$P_y / \rho gy' = -0.25 + 1.24\, y/h, \tag{14}$$

Left of middle block and straight joint:

$$P_y / \rho gy' = 2.24 - 1.27\, y/h, \tag{15}$$

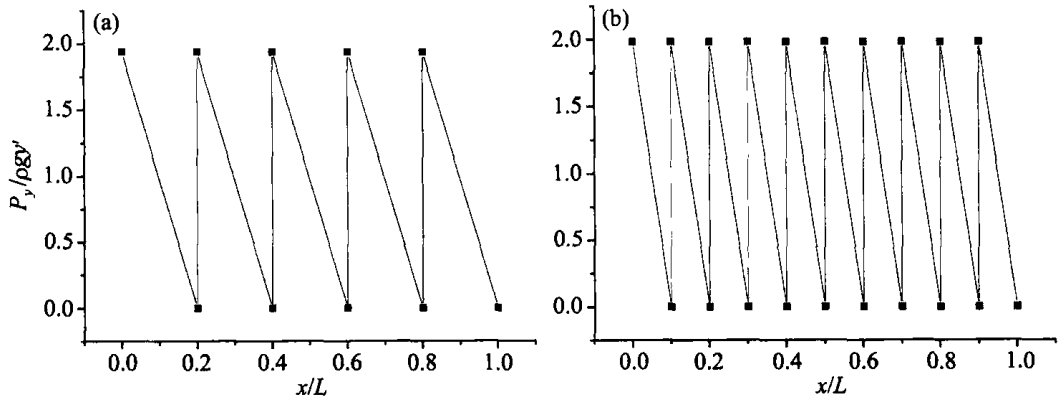

Fig. 6. Force distribution along sliding surface. (a) Big block and straight joints; (b) middle block and straight joints.

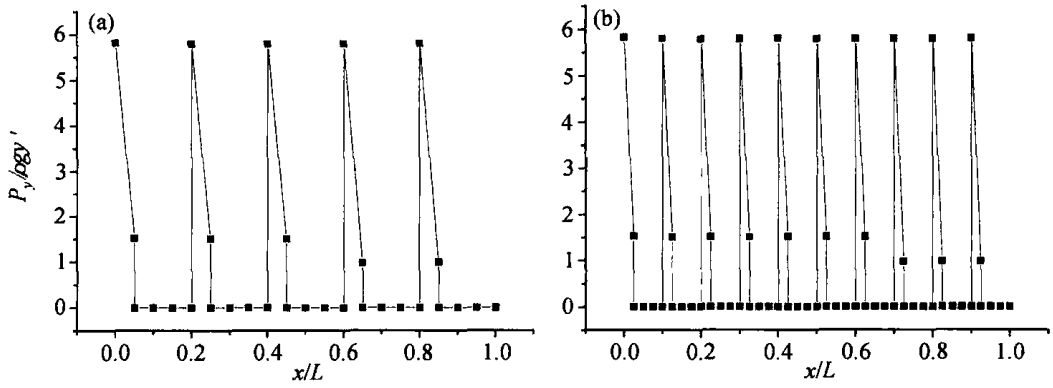

Fig. 7. Force distribution along sliding surface (smaller block division). (a) Big block and straight joints; (b) middle block and straight joints.

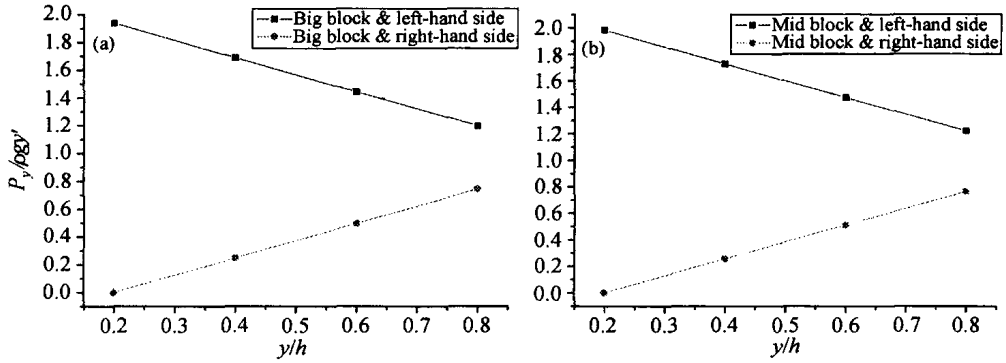

Fig. 8. Force distribution along vertical section. (a) Big block and straight joints; (b) middle block and straight joints.

Right of middle block and straight joint:

$$P_y / \rho g y' = -0.25 + 1.27\, y/h, \qquad (16)$$

$$0.2 < y/h < 0.8.$$

3.3 Slope with staged joints

(i) Failure modes. Figs. 9 and 10 are the failure modes obtained by numerical simulations and experimental observations. Experimental observations show that the sliding failure is the main mode for the slope of big blocks. The sliding begins from the upper layer and gradually propagates to lower layers due to the friction of upper layer. This observation is reproduced by the DEM as shown in Fig. 9(a). However, the slope of middle blocks has different failure mode although the main failure mode is still sliding. In this failure mode, the front column slides first and the subsequent column follows the sliding as shown in Fig. 10. The distance between columns becomes bigger and bigger from the front column. The DEM can reproduce this failure mode-column sliding, but cannot reproduce the bigger and bigger distance between columns.

(ii) Stress distribution along sliding surface and vertical section. Fig. 11 shows the force distribution along the sliding surface at critical angle. Figs. 9—11 show that $P_y/\rho g y'$ is small when x/L is small. This is because the slope is staged and the overburdened pressure at the bottom layer is small. The force reaches its maximum at the middle

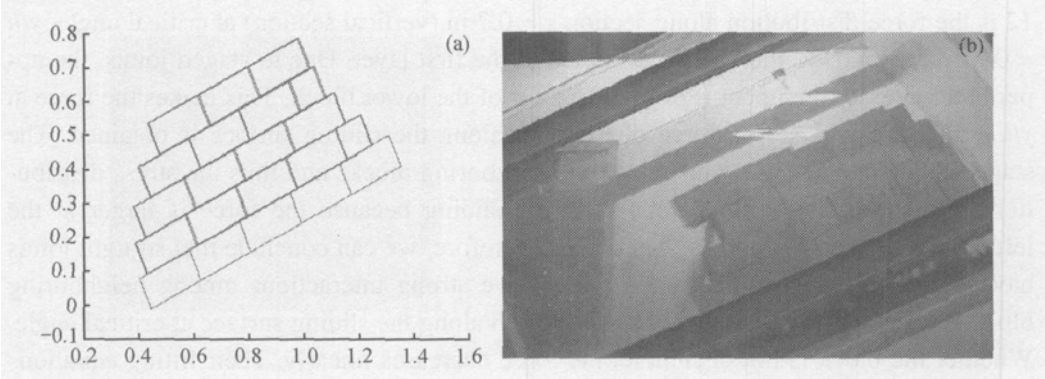

Fig. 9. Failure mode of slope with big blocks and staged joints. (a) DEM simulation; (b) experimental observation.

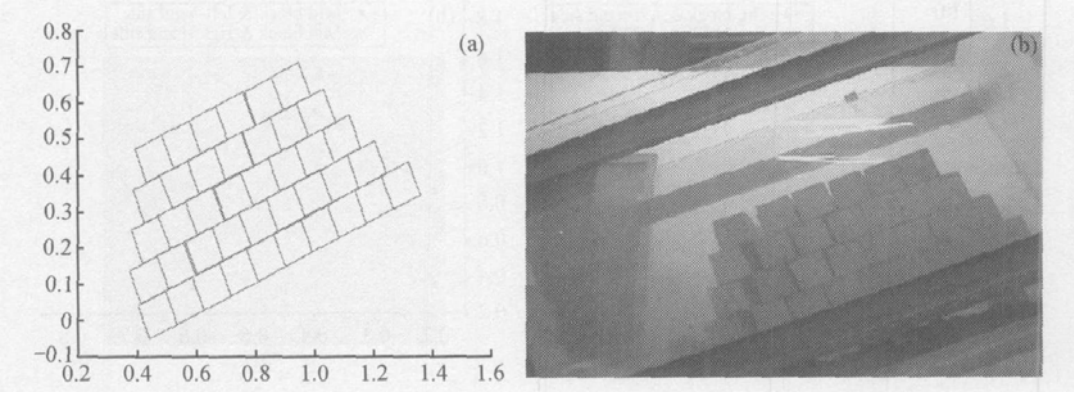

Fig. 10. Failure mode of middle blocks with staged joints. (a) DEM simulation; (b) experimental observation.

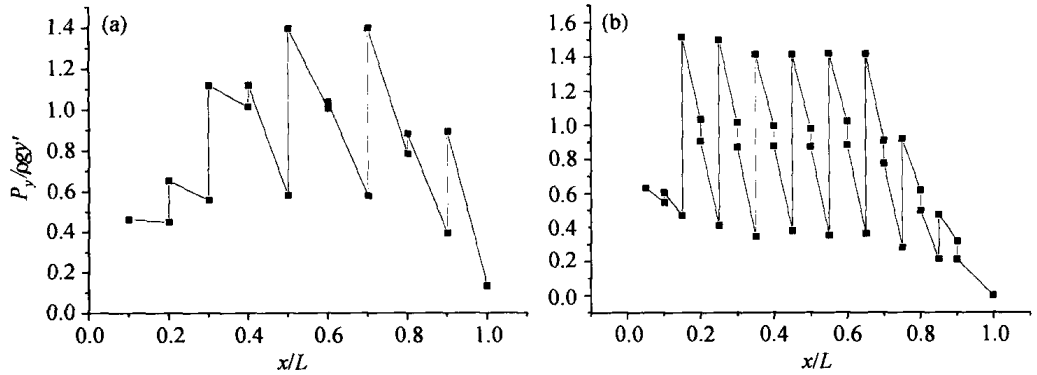

Fig. 11. Force distribution along sliding surface. (a) Big block and staged joints; (b) middle block and staged joints.

part and becomes small at the right corner. Therefore, for a large-scale slope, the normal force along the sliding surface is approximately homogeneous. If the strength of rock masses is homogeneous, the resistance should be homogeneous. Compared Fig. 6 with Fig. 11, it can be seen that the normal stress along the sliding surface is different, particularly at the two ends of the slope. This is due to different configurations of joints. Fig. 12 is the force distribution along section $x = 0.7$ m (vertical section) at critical angle. $y/h = 0.2$ corresponds to the contact interface of the first layer. Due to staged joints, the upper block presses the upper right-hand corner of the lower block. This makes the force at $y/h = 0.4$ larger. A sewed force distribution along the sliding surface is obtained. The staged joints increase the constraints on neighboring blocks and thus the stress distribution. Furthermore, the block rotates during sliding because the force is larger at the left-hand side than at the right-hand side. Therefore, we can conclude that straight joints have less interaction while staged joints have strong interactions among neighboring block columns. Fig. 13 is the force distribution along the sliding surface at critical angle. Whether the block is big or middle, the force decreases linearly. Their fitting equations are:

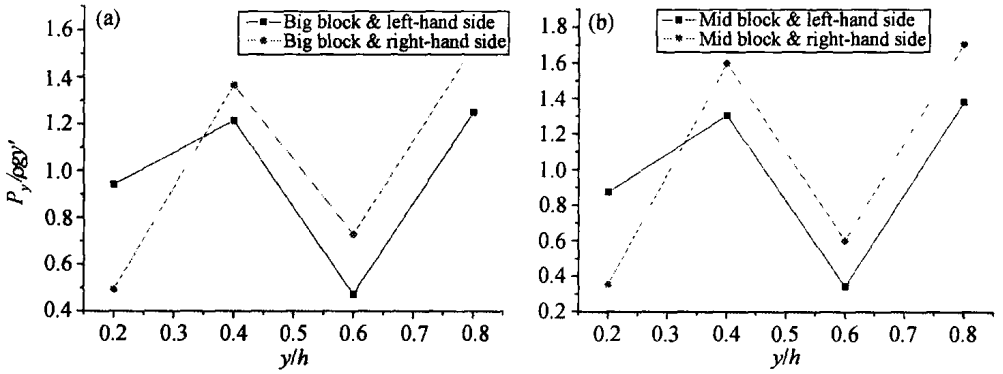

Fig. 12. Force distribution along vertical section. (a) Big block and staged joints; (b) middle block and staged joints.

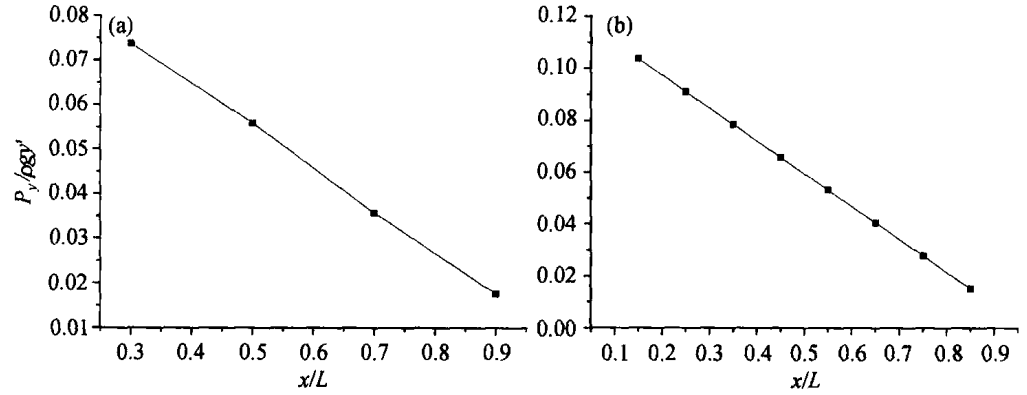

Fig. 13. Force distribution along sliding surface. (a) Big block and staged joints; (b) middle block and staged joints.

Big block and staged joint:

$$P_x = 0.102 - 0.094\frac{x}{L}, \quad 0.1 < \frac{x}{L} < 1; \tag{17}$$

Middle block and staged joint:

$$P_x = 0.123 - 0.127\frac{x}{L}, \quad 0.15 < \frac{x}{L} < 0.95. \tag{18}$$

The front angle of the slope changes with block size. The smaller the block is, the steeper the front angle, and the force transferred to the down-lower part is bigger. Therefore, the middle block has steeper decreasing than big blocks.

3.4 Analysis for mixed block slope

(i) Failure process. Fig. 14 is the failure process observed from both experiments and DEM simulation. Experimental observations reveal that the part of bigger blocks slides and the part of smaller blocks topples. This is a combined failure mode of sliding and toppling. The part of small blocks at the front first rotates, then the upper part of smaller slides, this presses the big block slides. The sliding of upper block induces the sliding of big blocks at the lower layers, producing the global failure of slope.

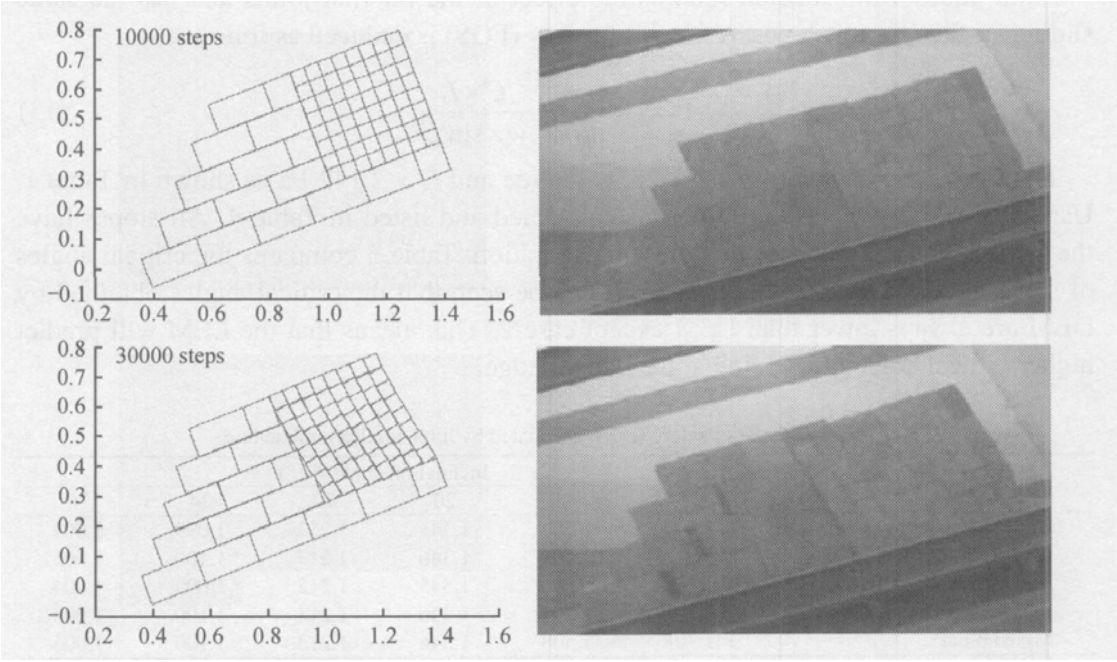

Fig. 14. Failure process of the slope with mixed blocks. Left is DEM simulation and right is experimental observation.

(ii) Force distribution along sliding surface and vertical section. Fig. 15 is the force distribution along the sliding surface. The left part is similar to the cases with staged joints while the right part is similar to the cases with straight joints. Fig. 16 is the force distribution along the x = 0.7 m section. The force at the left-hand side linearly decreases

up to zero at some height. This zero is due to the rotation of small blocks. However, the force at the right-hand side linearly increases with height and the contact at up-down blocks becomes more tightly with *y*/*h*.

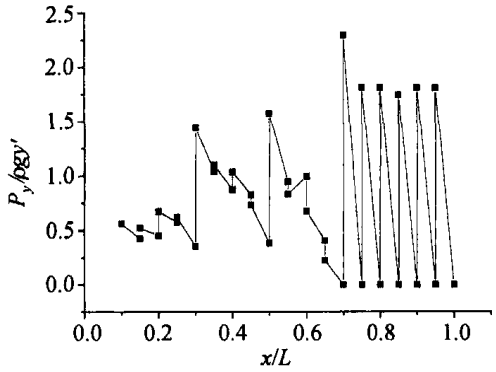

Fig. 15. Force distribution along sliding surface.

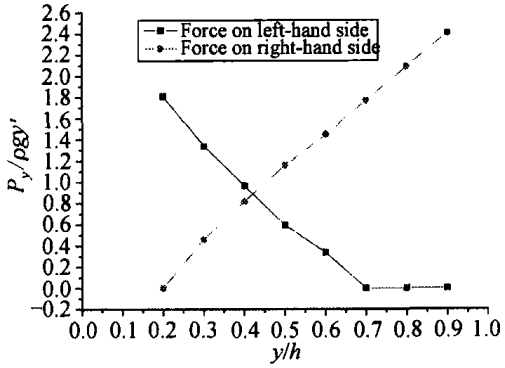

Fig. 16. Force distribution along vertical section.

4 Comparison of DEM with limit equilibrium method

4.1 Critical angle of slope

Limit equilibrium method ignores the effect of the internal joints and has the same sliding surface for all slopes. A factor of safety (FOS) is deduced as follows:

$$\mathrm{FOS} = \frac{\mathrm{tg}\phi}{\mathrm{tg}\beta} + \frac{C \times L}{w \times \sin\beta}. \tag{13}$$

The strength parameters are $\phi = 25.99$ degree and $C = 2.142$ Pa as shown in Table 1. Using these parameters, the FOSs was calculated and listed in Table 4. All slopes have the same FOS regardless of the joint configuration. Table 5 compares the critical angles of slope obtained by DEM and LEM. It can be seen that the critical angles obtained by DEM are always lower than LEM except case 2. This means that the LEM will predict higher critical angle, thus being at the danger edge.

Table 4 Factor of safety (FOS) calculated by limit equilibrium method

Experiment cases	Inclination angle β/(°)					
	16	18	20	22	24	26
Big block & straight joint	1.707	1.506	1.345	1.212	1.099	1.004
Big block & staged joint	1.708	1.508	1.346	1.213	1.100	1.005
Middle block & straight joint	1.707	1.506	1.345	1.212	1.099	1.004
Middle block & staged joint	1.708	1.508	1.346	1.213	1.100	1.005
Mixed block	1.708	1.508	1.346	1.213	1.100	1.005

Table 5 Comparison of failure angle between DEM and LEM

Methods	Case 1/(°)	Case 2/(°)	Case 3/(°)	Case 4/(°)	Case 5/(°)
LEM	26	26	26	26	26
DEM	23	25.5	10	23.5	21

4.2 Failure modes

Fig. 17 compares the failure modes obtained by both DEM and LEM simulations. For

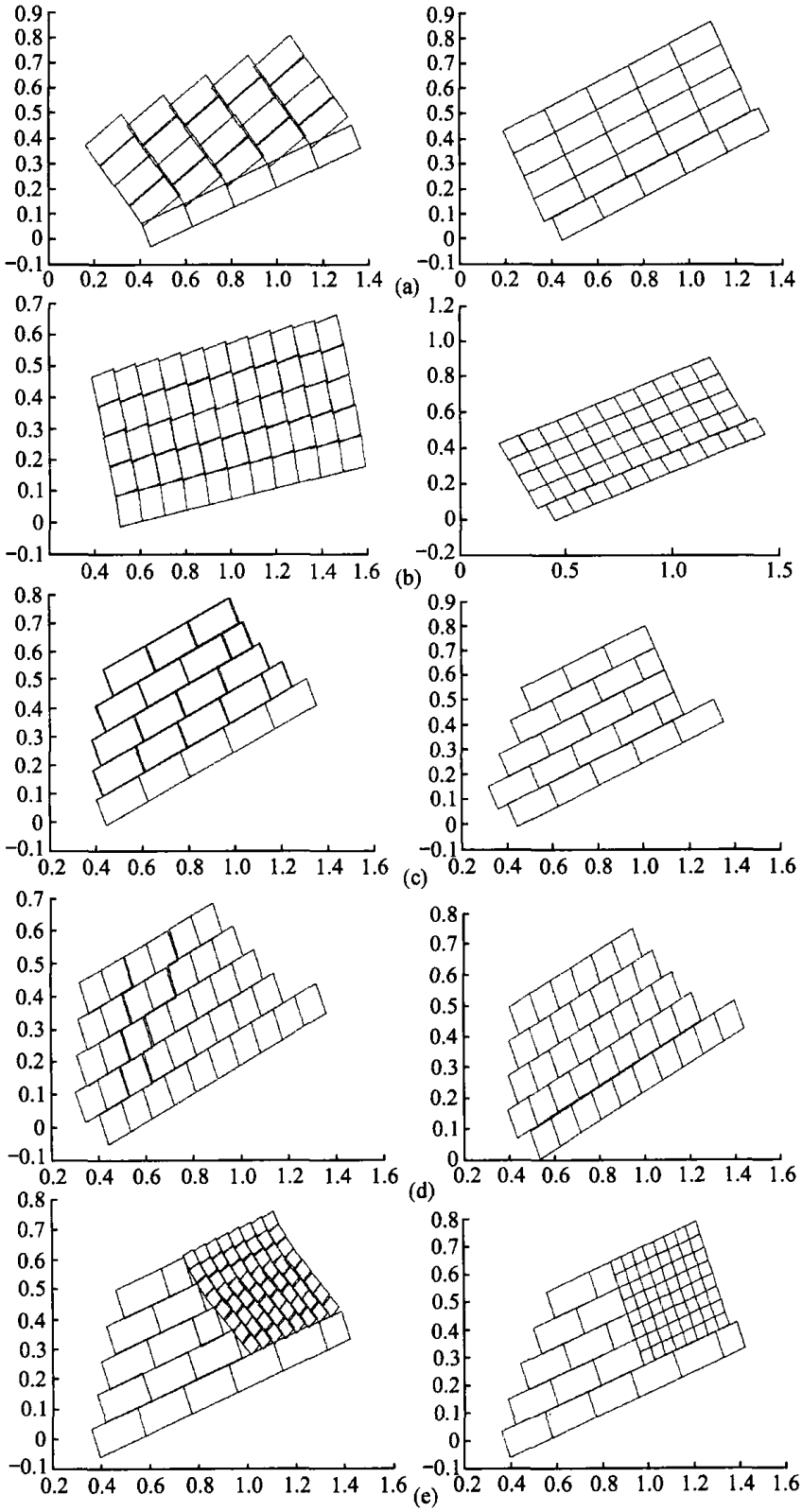

Fig. 17. Comparison of failure modes predicted by DEM and limit equilibrium method. Left is DEM result and right is limit equilibrium method result. (a) Big block and straight joints; (b) middle block and straight joints; (c) big block and staged joints; (d) middle block and staged joints; (e) mixed blocks.

the slope with straight joints, LEM predicts sliding mode while DEM predicts toppling mode. For the slope with staged joints, both LEM and DEM predict sliding modes. However, even though, their sliding displacements vary with layers. DEM predict higher displacements at the upper layers while LEM predicts the same displacements for all layers. For mixed slope, DEM predicts the sliding in big block part and toppling in small block part. However, LEM predicts only global sliding along the bottom-sliding surface.

5 Conclusions

This paper studied the effect of joint configurations and block size on the stability of rock slopes by using both DEM simulation and experimental observations. The failure modes and force distribution along sliding surface and vertical section were studied for five joint configurations. The DEM simulations were also verified with experimental observations. Finally, the failure mode and factor of safety were compared between DEM and LEM. From these studies, following conclusions and understandings can be drawn:

First, failure mode of jointed slope is not unique. Experimental observations show that failure modes have sliding, toppling, or their combination. The block size, joints distribution, and the mechanical properties of joints have vital effects on the failure development and failure modes.

Second, the DEM can accurately predict the critical angle of a slope for any joint configurations. The progressive failure from initial failure at local block to full failure at whole slope can be reproduced. The sliding and toppling failures causes the block rotating along the sliding surface. This causes inhomogeneous stress distribution along the sliding surface. The stress in each block is changing with slope angle. This adjustment depends on the joint configurations. For example, in the slope with straight joints, the stress decreases at the right-hand side while increases at the left-hand side of each block.

Third, the DEM can predict different failure modes while LEM can predict only sliding mode. For the slopes with staged joints, both DEM and LEM predict the sliding mode. However, the LEM cannot predict the toppling and fracturing failures. This is because the failures are progressive and starts from local failure. Because LEM cannot take the joint configurations into account, the factor obtained by LEM is higher. The DEM predictions are in good agreement with experimental observations.

Acknowledgements This work was supported by the Research Project of the Chinese Academy of Sciences (Grant No. KJCX2-SW-L1) and the National 973 Project (Grant No. 2002CB412703).

References

1. Cui Zhenquan, Li Ning, Slope Engineering—New Development of Theory and Practice (in Chinese), Beijing：China Water Conservancy and Water Electricity Publishing House, 1999.
2. Sun Guangzhong, Structural Mechanics of Rock Mass (in Chinese), Beijing: Science Press, 1988.
3. Chen Zhongyi, Zhou Jingxing, Wang Hongjing, Soil Mechanics (in Chinese), Beijing: Tsinghua University Press, 1994
4. Duncan, J. M., Factors of safety and reliability in geotechnical engineering, Journal of Geotechnical and

Geoenviromental Engineering, 2000, 126(4): 47－86.
5. Duncan, J. M., Limit equilibrium and finite element analysis of slopes, Journal of Geotechical Engineering, 1996, 122(7): 577－596.
6. Jing, L., A review of techniques advances and outstanding issue in numerical modeling for rock mechanics and rock engineering, Int. J. of Rock Mechanics & Ming Sciences, 2003, 40: 283－353.
7. Cundall, P. A., A computer model for simulating progressive，large scale movements in blocky rock systems, in Proc. of the Int. Symp. Rock Fracture，ISRM, Nancy, Paper No.II-8, Vol.1, 1997.
8. O'Connor, K. M., Dowing, C. H., Distinct element modeling and analysis of mining-induced subsidence, Rock Mechanics and Rock Engineering，1992，25: 1－2.
9. Dong Dapeng, Improved algorithm for a three-dimensional discrete element method and its application, Master Thesis, Chinese Academy of Science, Beijing, 2002.
10. Li Shihai, Zhao Manhong, Wang Yuannian et al., A new numerical method for DEM–block and particle model, Int. J. of Rock Mechanics & Mining Sciences, 2004, 41: 436.
11. Barla, G., Borri-brunetto, M., Gerbaudo, G., Fractured and Jointed Rock Masses (eds. Myer, L. R., Cook, R. E., Goodman, N. G. W., Tsang, C. F.), Rotterdam: Balkema, 1995.
12. Barla, G., Borri-brunetto, M., Validation of a distinct element model for toppling of rock slope, in 8th Int. Congress on Rock Mechanics, ISRM, Tokyo, 1995, Vol.3, 417－421.
13. Barla, G., Jing, L., DEM modeling of laboratory tests of block toppling, Int. J. Rock Mechanics & Mining Sciences, 1997, 34: 506－507.